in Modeling of Casting and Welding Processes, AIME, Warrendale, PA, 197, 1981.

MATHEMATICAL MODELING OF THE TEMPERATURE PROFILES AND WELD DILUTION IN ELECTROSLAG WELDING OF STEEL PLATES

T. Deb Roy, J. Szekely*, and T. W. Eagar*

Metallurgy Section
Department of Materials Science and Engineering
The Pennsylvania State University
University Park, PA 16802

*Department of Materials Science and Engineering
Massachusetts Institute of Technology
Cambridge, MA 02139

This paper describes a calculation procedure for the detailed prediction of temperature profiles and weld dilution in the electroslag welding of mild steel plates. The temperature profiles in the liquid slag and the liquid metal regions are calculated in three dimensions under steady state conditions. The values of the heat generation patterns needed in the temperature profile calculation are computed by solving a three dimensional electric field equation in the liquid slag region. The weld dilution is computed as a function of time by solving a transient three dimensional heat flow equation for the base plate.

Good agreement achieved between the predicted temperature profiles in the base plate and the available measurements illustrate the capabilities of the model. Reasonable agreement has also been obtained between the measurements and the predicted values of dilution as affected by changes in the plate gap and the weld speed.

Introduction

In recent years, the electroslag welding process has been a subject of growing interest to engineers and research scientists because of its potential attractiveness for the welding of thick plates. At present there is some reservation in the application of this fast and economical welding process for critical applications. In the current electroslag welding practice the size of the heat affected zone is relatively large and the fracture toughness of the welds is often poor.

The work described in this paper is a part of a research program aimed at developing a fundamental understanding of the heat and fluid flow phenomena in the electroslag welding process with the ultimate objective of providing guidelines for operation so as to achieve improved weld properties.

Most of the earlier work on the electroslag welding of steels was concerned with the physical characterization of the weld by examining its microstructure and by conducting other suitable tests to determine fracture toughness and other mechanical properties of the weld for a variety of welding conditions. Some examples of these studies are the papers by Paton,[1] Eagar and Ricci,[2] des Ramos, Pense and Stout,[3] Liby and Olson,[4] and by Jackson.[5] So far relatively less work has been done on the prediction of important weld characteristics such as the size of the heat affected zone, grain growth, and the weld dilution.

The first modeling work on the ESW process, presented by Dilawari, Szekely, and Eagar,[6] deals with the calculation of heat and fluid flow in the liquid slag and liquid metal regions in idealized two dimensional systems. It is found that the computed results are significantly influenced by the system geometry. Subsequently, a computation scheme has been presented[7] to calculate the temperature fields and the heat generation patterns in truly three dimensional systems. The work establishes that a reduction in the heat input, a crucial objective in the electroslag welding process, can be achieved by using narrow plate gaps or by using closely spaced multiple electrodes.

This previous paper,[7] while providing useful information (such as the effect of electrode asymmetry on the heat generation pattern) about the process, did not deal with some of the important aspects of the welding process, such as the weld dilution. Also, the temperature profiles were calculated for the liquid metal and the liquid slag regions only and the calculation of transient heat flow in the base place was not carried out.

These problems are addressed in the present paper. Some of the attractive features of the earlier computation scheme, such as the computation of heat generation patterns and temperature profiles in the liquid region in a truly three dimensional situation are retained in the present model. However, the computation has been extended to account for the three dimensional transient heat flow in the base plate and the weld dilution.

In the following sections, we shall outline the mathematical model and the computational procedure. This is followed by a section on the comparison between the computed results and the available experimental data and the conclusions from this study.

Mathematical Modeling

In the electroslag welding system, a diagram of which is shown in Figure 1, the current passes through the consumable electrode, through the molten slag, to the base plate, either directly or indirectly through the molten metal pool. This results in the establishment of voltage profiles and spatially distributed heat generation patterns in the liquid slag. As a result of the heat generation, the consumable electrode melts, forming a pool of liquid metal underneath the liquid slag. The solidification of the liquid metal pool forms the weld. The nonuniform current density in the slag results in the establishment of an electromagnetic force field which causes circulation in the liquid region. Heat generated in the liquid slag is transported to the base plate by conduction and by convection. Part of this heat is utilized for the melting of the base plate and is responsible for the weld dilution while the remainder is transferred into the base plate and is responsible for the thermal cycle in the base plate, the establishment of a heat affected zone, and the resultant grain growth.

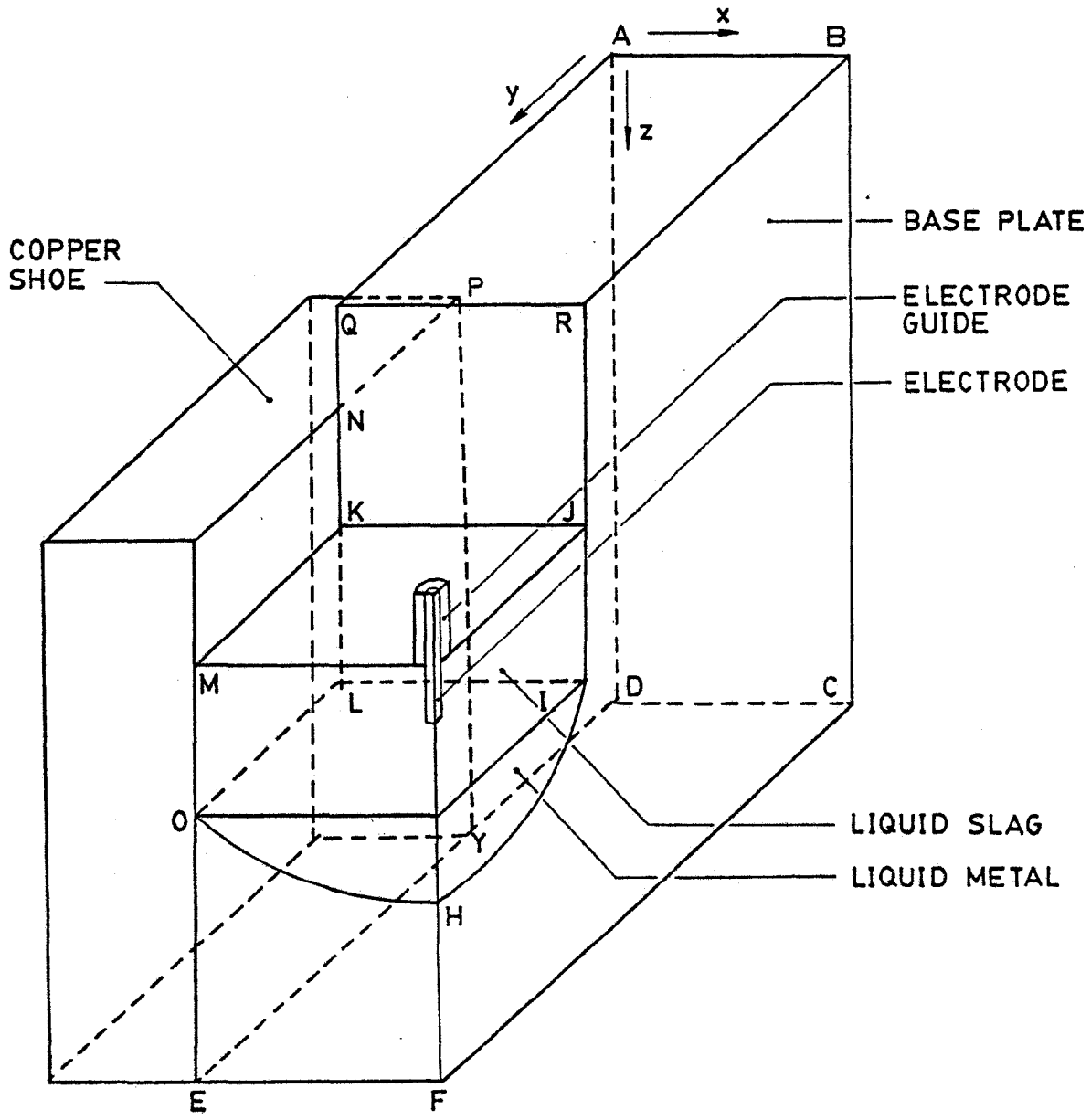

Figure 1. Sketch of the ESW Process

The following physical processes are to be considered in order to simulate the welding process:

(a) The passage of current from the electrode through the molten slag and metal pools to the base plate results in the establishment of a spatially distributed heat generation pattern.

(b) Heat transfer in the liquid metal and liquid slag takes place by conduction, convection, and by the transport of the liquid metal drops from the slag to the metal phase.

(c) Thermal energy is transferred in the base plate by transient conduction and the time dependent position of the boundary separating the molten and the solid metal regions is determined by a dynamic heat balance.

The calculation procedure adopted here for the detailed prediction of heat generation patterns and temperature profiles in the liquid region of the electroslag welding process has been presented recently.[7] In short, the modeling equations are represented by statements of the appropriate electric field equations together with Ohm's law in three dimensions in order to calculate the spatially distributed heat generation pattern. The heat generation pattern is calculated only for the liquid slag phase since the electrical resistance of the slag phase is several thousand times higher than that of the metal phase and practically all of the heat is generated in the slag phase. Having calculated the heat generation patterns for the liquid slag, attention is focused on the calculation of the temperature profiles in the liquid slag and liquid metal. Estimates of the temperature profiles are made by solving the heat flow equations using effective thermal conductivities to account for the convection in the liquid metal and liquid slag phases. The calculation scheme[7] accounts for the transport of heat from the slag to metal phase by the liquid metal drops, the energy loss due to electrolysis, and the energy required for the heating of the cold slag charge.

The temperature profile in the base plate is represented by the following relationship:

$$\nabla(k\nabla T) = \rho C_p \frac{\partial T}{\partial t} \qquad (1)$$

The boundary conditions used for the solution of the above equation are presented in Appendix A. It is noted that both the thermal conductivity and the specific heat are allowed to be temperature dependent, but this temperature dependence is determined solely by the nature of the material.

In the present computation the property values for low carbon steel are used and the following relationships are employed to describe the temperature dependence of the thermal conductivity,[8] and the specific heat.[9]

$$\begin{aligned} k &= 9.2 \times 10^{-2} - 5.86 \times 10^{-5} T \quad \text{for } T < 1050 \text{ K} \\ &= 3.05 \times 10^{-2} \qquad\qquad\qquad\quad \text{for } T > 1050 \text{ K} \end{aligned} \qquad (2)$$

k is expressed in kW/mK

$$\begin{aligned} C_p &= 0.46 + 4.18 \times 10^{-4} T \quad \text{for } T < 1000 \text{ K} \\ &= 0.88 \qquad\qquad\qquad\quad \text{for } T > 1000 \text{ K} \end{aligned} \qquad (3)$$

C_p in the above equation is expressed in kW/kgK

The melting rate of the base plate can be calculated from the following equation:

$$m_b = (Q_{s\ell p\ell} - H_{s\ell p\ell})/\Delta H \quad (4)$$

where $Q_{s\ell p\ell}$ and $H_{s\ell p\ell}$ (in kW) are the rate of heat transfer from the liquid slag to the base plate and the rate of heat transfer from the melting base plate to the interior of the base plate. These quantities are calculated from the temperature field by integrating the local values of heat fluxes, and ΔH is the latent heat of fusion in kJ/kg. The amount of base metal dilution is readily obtained from the following expression:

$$\% \text{ Dilution} = m_b/(m_b + m) \quad (5)$$

where m is the electrode melting rate calculated during the heat flow calculation in the liquid slag region.[7]

Computational Method

Tasks

The computational scheme described in the present section is designed to perform the following tasks:

(1) Solution of the electric field equation in the slag phase to calculate the voltage profiles and heat generation patterns in three dimensions.

(2) Solution of the steady state, three dimensional heat flow equations in the liquid regions with due consideration for the transport of heat from the slag to the metal phase by the liquid metal drops, the energy loss due to electrolysis, and the energy required for the heating of the cold slag charge.

(3) Calculation of the three dimensional temperature profiles in the base plate as a function of time by solving a transient heat conduction equation.

Sequence of Operations

As has been discussed earlier, the electric field equations and the heat flow equations are not explicitly coupled. The calculation of the temperature profiles in the liquid slag and the liquid metal regions requires knowledge of the heat generation pattern which in turn requires solution of the electric field equation in the slag region. However, the physical dimension (width) of the region is not known a priori since the width of this region is related to the weld dilution--a quantity which can be calculated only after the heat flow equations are solved for the liquid regions and for the base plate. Therefore, an iterative computational scheme, outlined in Figure 2, has been adopted.

In short, an iterative scheme is used in which the computation is started with an assumed value of dilution. The electric field equation and the modified heat conduction equations in the liquid regions are solved

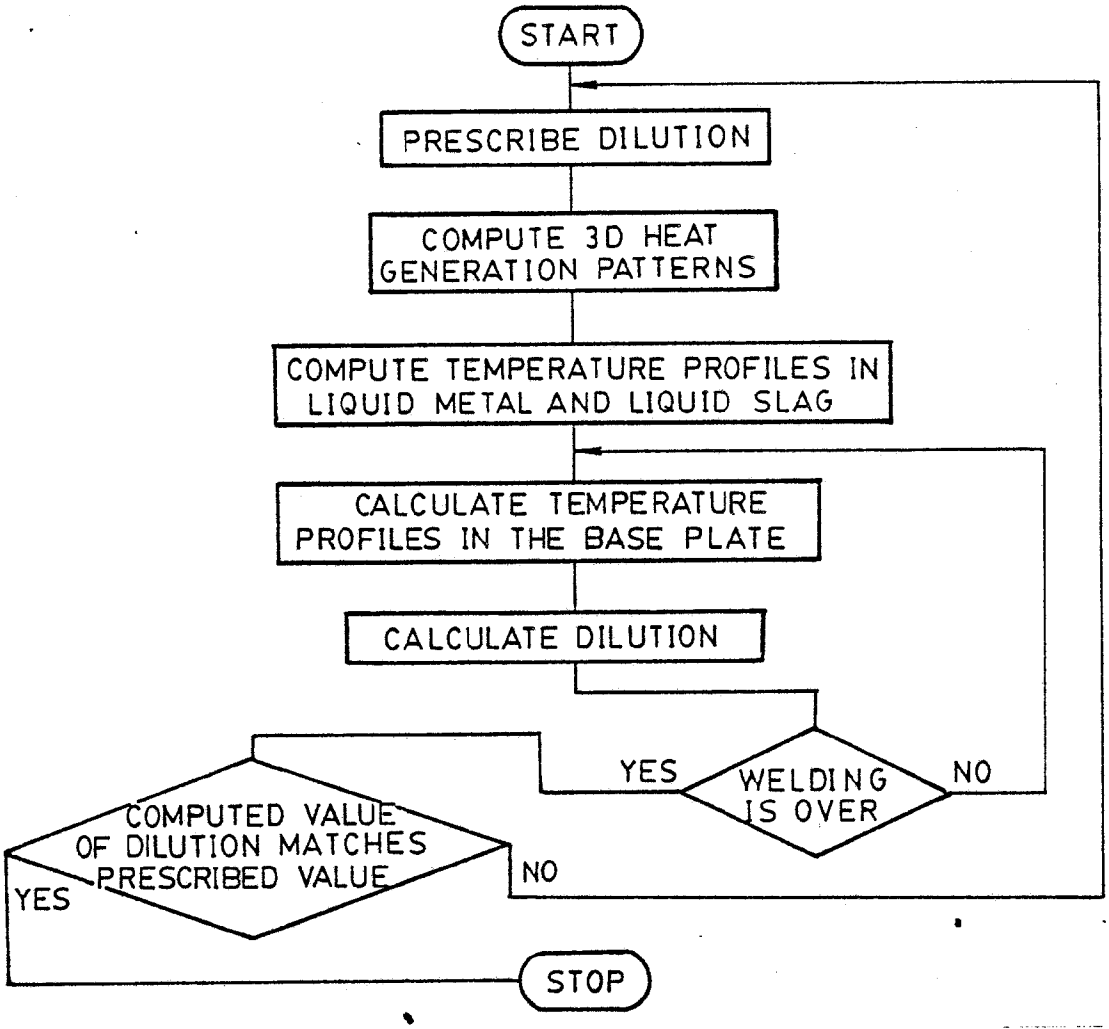

Figure 2. Schematic flow sheet of the computer program

sequentially. This is followed by the solution of the transient heat conduction equation for the base plate to compute the temperature profiles and the weld dilution as a function of time. The time average value of the weld dilution is then compared with the initially assumed value of dilution. The procedure is repeated until the assumed and the computed values of weld dilution agree within 2%.

Details of the Computational Work

Use of Effective Conductivity. In the present computations effective or enhanced values of thermal conductivity are used for the computations relating to the bulk of the liquid slag and the liquid metal phases. Near the solid walls (grid nodes closest to the solid walls) relatively lower values of effective thermal conductivity presented in Table I are used. The effects of using different values of effective conductivity have been examined in our earlier paper.[7] In the present computations, the near wall values are used only for the grid nodes next to the solid walls.

Grids. The electric field equation and the heat flow equations are solved in finite difference forms using nonuniformly spaced rectangular grids. Irregular boundaries are approximated by judicious choice of grids.

Table I. Values of Effective Thermal Conductivity (kcal/mKs)

	bulk	near wall
slag	0.6	0.075
metal	0.3	0.15

For example, the circular cross section of the electrode is represented by a regular octagon, The locations of the grid nodes are presented in Table II.

Table II. Details of the Finite Difference Grid Distribution

Direction	Location (cm)
Grids in the Liquid Region	
x	0, 0.05, 0.18, 0.34, 0.50, 0.66, 0.83, 1.0, 1.08, 1.15, 1.23, and 1.27 (12 nodes)
y	60.3, 60.38, 60.54, 60.82, 61.1, 61.38, 61.66, 61.94, 62.22, 62.38, 62.46, and 62.5 (12 nodes)
z	0, 0.2, 0.63, 1.07, 1.51, 1.94, 2.37, 2.80, 3.0, 3.2, 3.5, 3.8, 4.1, 4.4, and 4.5 (15 nodes)
Fixed Grids in the Base Plate (cm)	
x	0, 0.16, 0.48, 0.80, 1.12, and 1.27 (6 nodes)
y	0, 15.0, 35.0, 44.0, 50.0, 53.95, 55.22, 56.49, 57.12, 57.76, 58.4, 59.03, 59.48, 59.85, 60.10, 60.30, 60.80, 61.40, 62.00, and 62.50 (20 nodes)
Examples of Time Dependent Flexible Grid Locations in the z-Direction (cm)	
t = 203 s	0, 5.6, 11.4, 17.1, 22.8, 28.5, 34.2, 36.9, 39.3, 39.9, 41.1, 42.3, 42.9, 43.8, 44.4, 44.9, and 45.8 (17 nodes)
t = 390 s	0, 5.6, 11.4, 17.1, 22.8, 28.5, 31.2, 33.6, 34.2, 35.4, 36.6, 37.2, 38.1, 38.7, 39.2, 39.9, and 45.8 (17 nodes)

In the base plate, temperature variations are maximum in the vicinity of the base plate/liquid slag interface. To achieve a reasonably high accuracy in the computations, closer grid spacings are needed in the vicinity of the melt/solid boundary. This is achieved by choosing

sufficiently small grid sizes (nonuniformly spaced, fixed) in the x and y directions (in the horizontal plane) and by using time dependent flexible grid locations in the vertical z-direction (welding direction). Since the welding speed is related to the electrode melting rate and is calculated prior to the computations in the base plate, the z-location of the top of the slag surface can be determined with reference to a fixed origin at any given time. During the computations, the time steps are calculated in such a manner than the top of the slag surface coincides with one of nine, fixed predetermined locations in the z-direction. In addition to these nine grids, eight flexible grids are stationed on both sides of the "top slag surface"--two of these being above this surface and six below it. The total number of working grids at any given time in the z-direction was, therefore, 17 stationed flexibly with due consideration to the location of the plane representing the top slag surface, The locations of the working z-grid nodes in the base plate at two time instances are presented in Table II, along with the locations of the x and y nodes in the base plate.

The total number of grids at any given time is, therefore, 6 x 20 x 17 = 2040 in the base plate and 12 x 12 x 15 = 2160 in the liquid region. A typical calculation takes about 500 sec of central processing time on MIT's IBM 370 digital computer.

Solution of the Finite Difference Equations. The finite difference equations are solved by an iterative scheme involving a line-by-line solution procedure. The scheme known as tridiagonal matrix algorithm (TDMA) is a particular version of Gaussian elimination technique in which the values of a variable, such as voltage or temperature at all the grid points on a line, can be updated at a time. This method is appreciably faster than the point-by-point iteration scheme in which the value of a variable is updated only at a single grid node. To achieve fast convergence, the algorithm TDMA is used in the vertical direction where the variation in the value of a variable such as the voltage is significant. The computation starts with some assumed values of a variable at all the grid nodes. The assumed values are then updated along a chosen line and the boundary conditions are applied at both ends of the line. Once TDMA is applied for a line adjacent to a boundary surface, variable values on the nearest vertical line on this surface are updated by applying the appropriate boundary condition. After one cycle of iteration, the absolute values of the difference between the "old" and the updated values of the variable at all grid nodes are compared with a certain prescribed small quantity to check for the convergence. For the voltage calculations needed to compute heat generation patterns, the maximum allowable difference $|\phi - \phi_{old}|$, is prescribed to be less than 0.00001 volt. This specified difference in voltage amounts to only 0.00025% of the voltage difference between the electrode and the base plate. The accuracy of the computations is also ensured by means of independent checks. For example, for the voltage calculations, the numerically integrated value of heat generation pattern over the 3D region is compared with the product of the overall current and the voltage difference between the electrode and the base plate. For the calculation of temperature profiles, a maximum difference of 0.01 K was used as a convergence criteria to ensure sufficient accuracy in computations.

Computed Results and Discussion

The computed results provide information on the spatially distributed heat generation patterns, on the temperature fields in the molten regions, on the temperature fields within the base plate, and on the weld dilution.

In the model, the spatially distributed heat generation pattern is calculated by solving the electric field equation and is not taken as an adjustable parameter. A detailed study of the heat generation patterns and the temperature profiles in the liquid metal has been presented in an earlier paper.[7] The modeling work presented in this paper is an extension of the earlier work. Here the temperature distribution in the base plate has been treated as a transient three dimensional problem. The weld dilution is accounted for in the computations. The computed values of the temperature profiles and the weld dilution are compared with the available experimental data.

The data used for the computations are the typical values of different parameters encountered for the ESW of mild steel plates. These are presented in Table III.

Table III. Values of Various Parameters Used for the Calculation of Temperature Fields

Plate thickness	2.54×10^{-2} and 5.08×10^{-2} m
Initial plate gap	1.9×10^{-2} m & 3.0×10^{-2} m
Width of copper shoe	1.02×10^{-1} m
Electrode radius	1.2×10^{-3} m
Metal drop radius	1.2×10^{-3} m
Depth of the slag pool	3.0×10^{-2} m
Electrode immersion in the slag	1.5×10^{-2} m
Length of the base plate	0.30 and .61m
Electrode voltage	37V
Current	calculated in the program, roughly 500A
Molten slag electrical conductivity	$375\ (\text{ohm.m})^{-1}$
Molten slag thermal conductivity	1.05×10^{-3} kJ/(ms ^{o}K)
Molten metal thermal conductivity	2.1×10^{-2} kJ/ms ^{o}K)
Heat transfer coefficient at the slag/cooling shoe interface	1.67 kJ/m^{2}s ^{o}K)
Heat transfer coefficient at the base plate/cooling shoe interface	0.13 kJ/(ms^{o}K)
Convective heat transfer coefficient at the base plate surfaces	0.084 kJ(ms^{o}K)
Specific heat of the electrode	0.84 kJ/kg
Specific heat of the liquid metal drops	0.84 kJ/kg
Specific heat of the slag	1.05 kJ/kg
Latent heat of fusion of the electrode	272 kJ/kg
Emissivity of the free slag surface	0.6
Viscosity of the slag	1.0×10^{-2} kg/(ms)
Density of the liquid metal	7×10^{3} kg/m^3
Density of liquid slag	2.7×10^{3} kg/m^3

In the base plate transient three dimensional temperature profiles are calculated. Since the quantity of the data generated is voluminous, only a representative selection is presented here. However, the computer isotherms exhibit the typical behavior expected from a moving distributed heat source, the strength of which is calculated by solving electric field equations.

In Figure 3, the computer values of temperature at two different monitoring locations is shown as a function of time for the experimental conditions reported by Benter, et al.[10] Their experimental data are also presented in this diagram to enable a direct comparison between the predictions

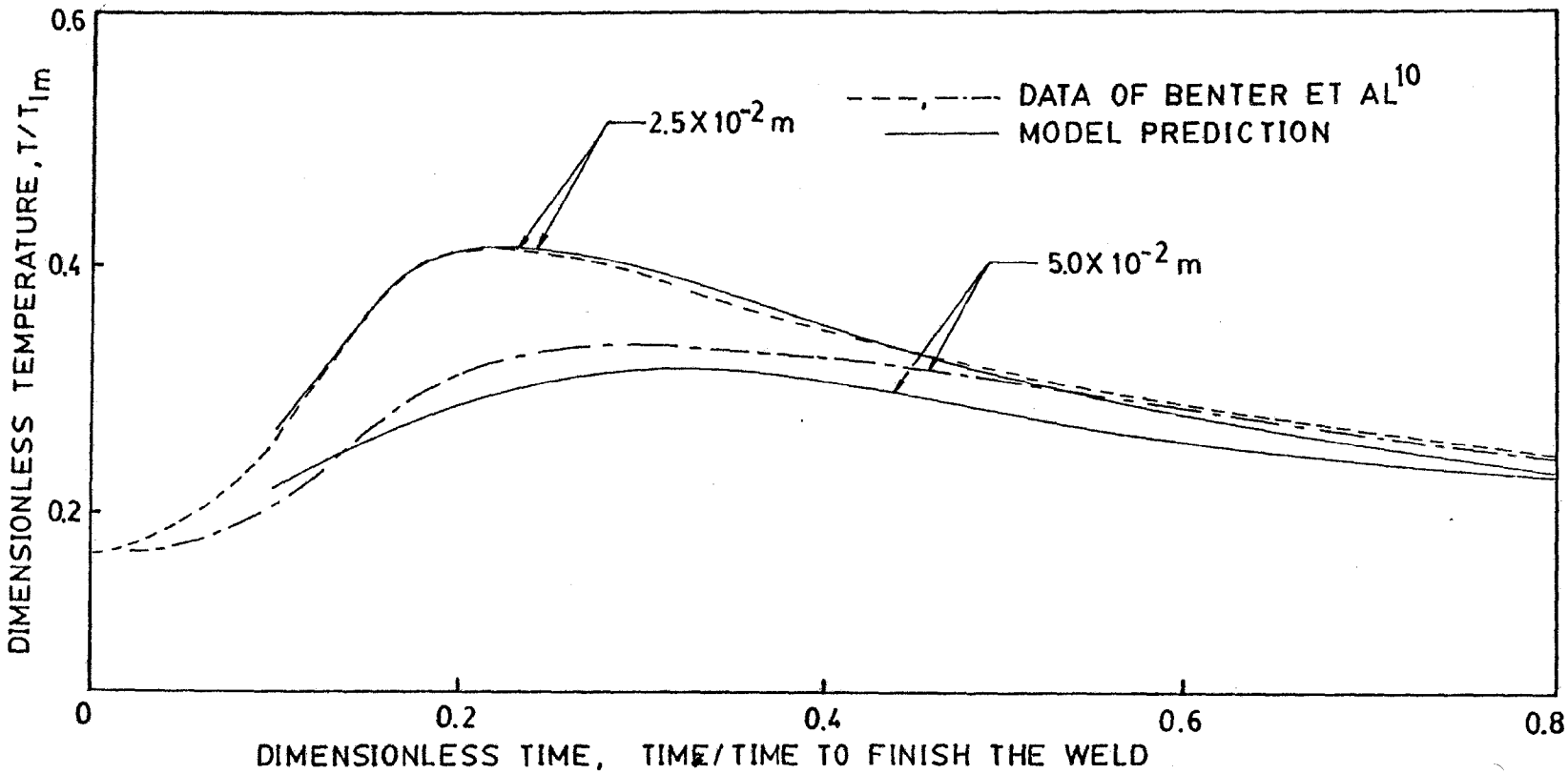

Figure 3. Temperatures at Monitoring Locations vs. Time. Monitoring locations are at the half thickness mid-sections near the bottom end of the base plate at distances from the weld face indicated on the graphs. Plate dimensions: 0.47m long, 0.61m wide, and 0.02m thick. Welding voltage = 37V, Plate gap = 0.03m, Electrode immersion = 0.015m. Welding speed = 3.1 x 10^{-4}m/s.

based on the model and the measurements. It is noted that the model did not incorporate the effect of the starting tab and, for this reason, one minute "starting delay" was made to represent this phenomenon.

Inspection of Figure 3 shows very good agreement between the predictions and the measurements.

The transient temperature profiles in the base plate establish the size of the heat affected zone and influence the grain growth in this region. Both these parameters are important in determining the mechanical properties of the weld. The roles played by different process parameters on the size of this zone and the grain growth phenomena are being studied at this time and will be reported in due course. However, it is seen from Figure 3 that relatively high temperatures are achieved at one inch distance from the welding face of the plate at the botton end of the vertical mid-section. Since the size of the heat affected zone is thought to be related to the peak temperature, the relatively high temperature value at the said monitoring location is consistent with a relatively large size of the heat affected zone commonly encountered in the ESW process. Furthermore, the data shown in Figure 3 underline the fact that electroslag welding is a transient process which has two important implications. One of these is that the properties of the weld may exhibit significant spatial variations; the other is that great care has to be taken in the selection of the test piece geometry, in order to reproduce faithfully the conditions in production scale operations.

As noted in the earlier section, the weld dilution is computed iteratively. The weld dilution and the solidification profile define the weld form factor, an important parameter in determining the weld quality. For this reason, it is of interest to examine the implications of the computer results regarding the weld dilution.

Figure 4 shows a plot of the percentage dilution, defined earlier in Eq. (5), against a dimensionless time. It is seen that initially the dilution is low, it attains a more-or-less steady value over a major length of the weld, and finally the dilution increases as the top of the plate is being approached. This behavior seems reasonable because during the initial stages most of the thermal energy is being used to preheat the plate, while a quasi-steady type heat balance is being maintained subsequently in the process, corresponding to the horizontal part of the curve. It is noted that the initially low level of dilution is usually compensated for, by using a starting tab.

Figure 5 shows a selection of experimental data reported by Benter et al,[10] relating the percentage dilution to the weld speed. It is seen that the data exhibit appreciable scatter; this is in part attributable to the difficulties in assessing dilution accurately; moreover the data represent measurements taken from several sections. The data indicate that dilution tends to decrease slightly, with increasing welding speed. The full line represents predictions based on the model, which seems to be in reasonable agreement with the measurements.

Figure 6 shows experimental measurements of Ricci[2] concerned with the effect of the plate gap on the percentage dilution. The theoretical predictions based on the model are also shown for the sake of comparison.

Here again the experimental measurements do exhibit appreciable scatter; nonetheless the predictions based on the model seem to be in reasonable agreement with the measurements.

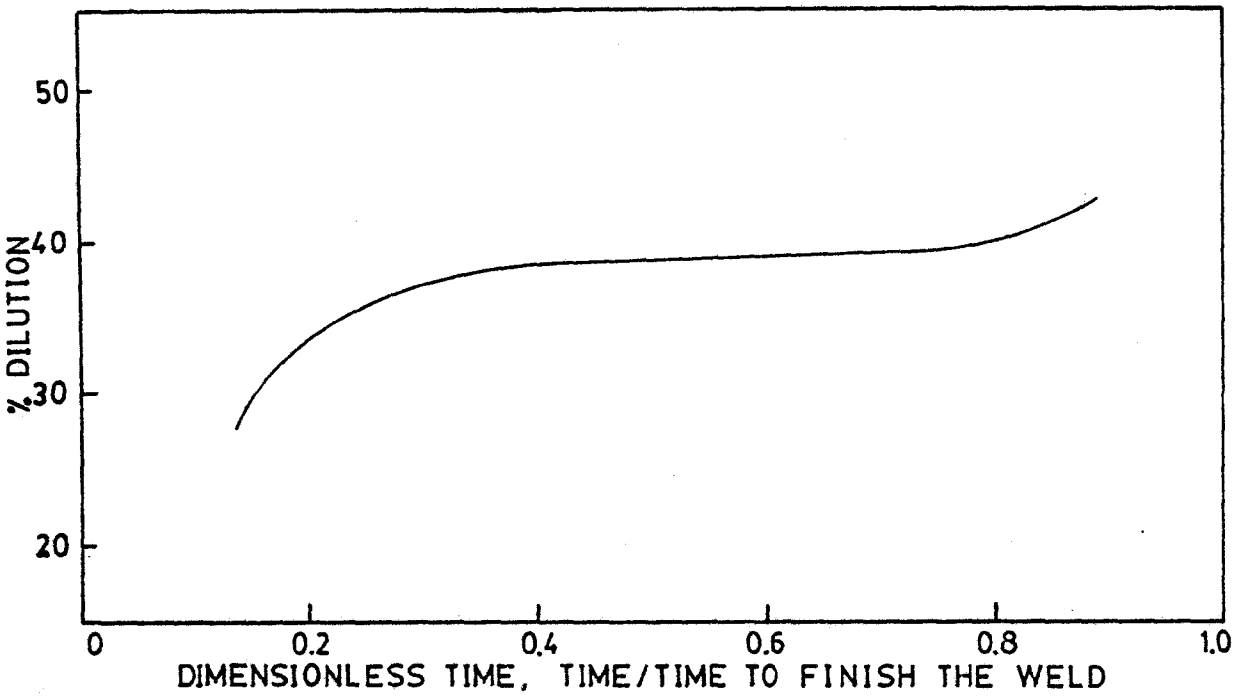

Figure 4. Dilution vs. Time. Plate dimensions = 0.47m long, 0.61m wide, and 0.025m thick. Welding voltage = 37V, Plate gap = 0.03m, Electrode immersion = 0.015m. Weld speed = 3.1×10^{-4}m/s.

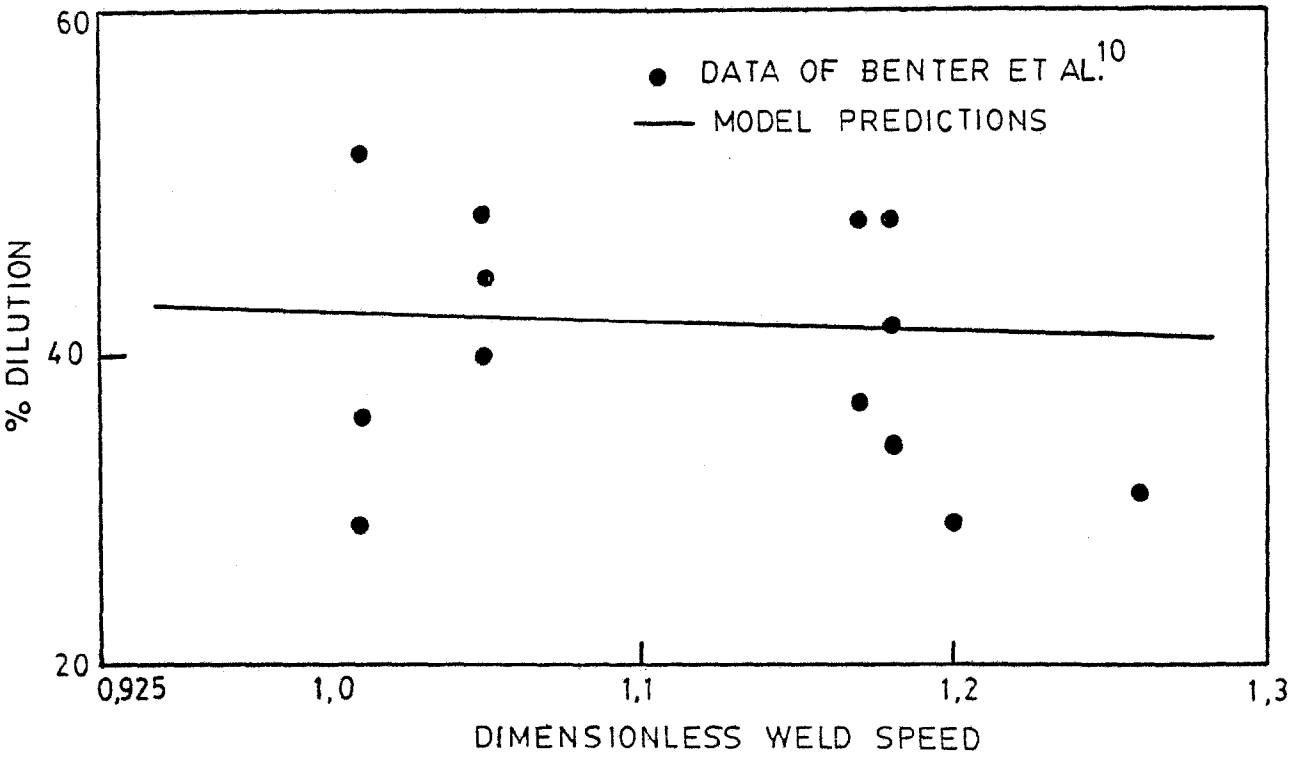

Figure 5. Dilution vs. Dimensionless Weld Speed. Plate dimensions: 0.47m long, 0.61m wide, and 0.025m thick. Welding voltage = 37V, Plate gap = 0.03m. Electrode immersion = 0.015m. Reference weld speed = 3.1×10^{-4}m/s.

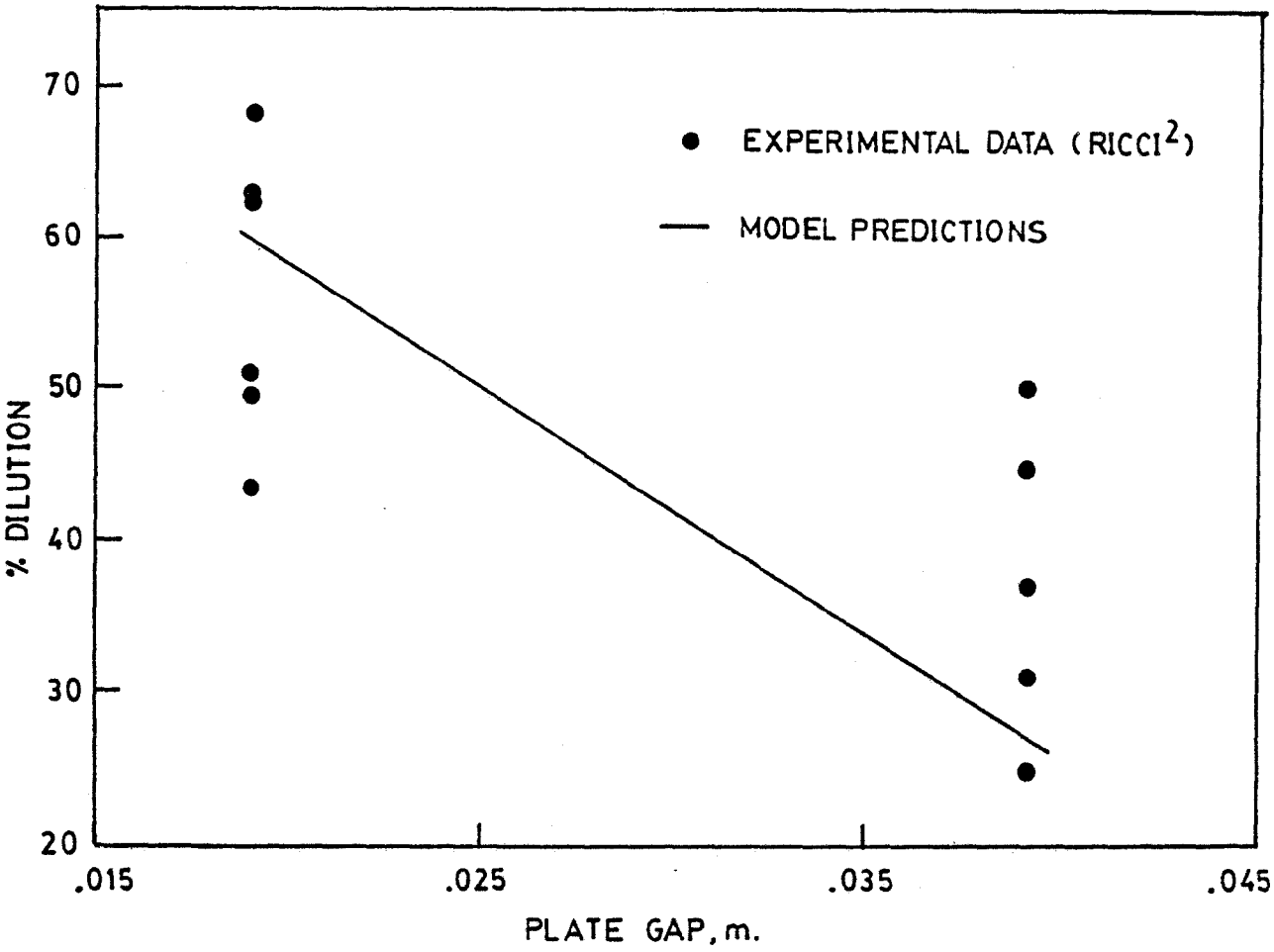

Figure 6. Dilution vs. Plate Gap. Plate dimensions: 0.3m long, 0.3m wide, and 0.05m thick. Welding voltage = 45V, Electrode immersion = 0.095m.

Conclusions

A mathematical representation of the ESW process has been used to compute the transient three dimensional temperature profile in the base plate and the weld dilution. The computed values of these quantities are found to be in good agreement with the available experimental data. The computed results indicate that electroslag welding is a transient process and that the properties of the weld may exhibit significant spatial variation. The weld dilution is found to be influenced by both the plate gap and by the weld speed. The dilution increases strongly with a decrease in the plate gap and increases mildly with a decrease in the weld speed.

References

1. B. E. Paton, Electroslag Welding, American Welding Society, New York, 1962.

2. Private communication, T. W. Eagar and W. S. Ricci, Department of Materials Science and Engineering, MIT, Cambridge; also W. S. Ricci, M.S. Thesis, MIS, September 1979.

3. J. B. des Ramos, A. W. Pense, and R. D. Stout, "Fracture Toughness of Electroslag Welded A 5376 Steel," Welding Journal Research Supplement, 55 (1) (1976) pp. 1-s to 4-s.

4. A. L. Liby, D. L. Olson: "Metallurgical Aspects of Electroslag Welding: A Review," Quarterly of the Colorado School of Mines, V 69 (1974).

5. C. E. Jackson: "Fluxes and Slags in Welding," Bulletin No. 190, Welding Research Council, December 1973.

6. A. H. Dilawari, J. Szekely, and T. W. Eagar, "An Analysis of Heat and Fluid Flow Phenomena in Electroslag Welding," Welding Journal, January 1978, p. 245.

7. T. Deb Roy, J. Szekely, and T. W. Eagar, "Heat Generation Patterns and Temperature Profiles in Electroslag Welding," accepted for publication in Metallurgical Transactions, B.

8. Y. S. Touloukin, et al, Thermal Conductivity, Metallic Elements and Alloys, Thermophysical Properties of Matter, IFI/Plenum, NY 1970.

9. Y. S. Touloukin, et al, Specific Heat, Metallic Elements, and Alloys, Thermophysical Properties of Matter, IFI/Plenum, Ny 1970.

10. W. P. Benter, Jr., P. J. Konkol, B. M. Kapadia, A. K. Shoemaker, and J. F. Sovak, Acceptance Criteria for Electroslag Weldments in Bridges, Phase I. Final Report, U.S. Steel Corporations, April 1977.

Acknowledgement

The authors gratefully acknowledge the support from the Department of Energy under contract No. ER-78-S-02-4799.A001.

APPENDIX A

Boundary Conditions for the Calculation of Temperature Profiles in the Base Plate

The following boundary conditions are used for the computation of temperature profile in the base plate. Figure 1 shows the different places mentioned in this section.

(i) Vertical surface of the plate, ABCD plane:

$$k \frac{\partial T}{\partial y} = h_c(T - Ta) \tag{A1}$$

(ii) Bottom end of the plate, CDEF plane:

$$-k \frac{\partial T}{\partial z} = h_c(T - Ta) \tag{A2}$$

(iii) Mid-section symmetry plane, RJI HFCB plane:

$$\frac{\partial T}{\partial x} = 0 \tag{A3}$$

(iv) Plate-cooling shoe interface, PYEOLN plane:

$$k \frac{\partial T}{\partial x} = h_c(T - Ta) \tag{A4}$$

(v) Vertical surface of the plate, ADYPNQ plane:

$$k \frac{\partial T}{\partial x} = h_c(T - Ta) \tag{A5}$$

(vi) Top surface of the plate, ABRQ plane:

$$k \frac{\partial T}{\partial z} = h_c(T - Ta) \tag{A6}$$

(vii) Mid-section symmetry plane, EFHO plane:

$$\frac{\partial T}{\partial y} = 0 \tag{A7}$$

(viii) The curved surface at the liquid metal/plate surface, OLIH plane:

$$T = T_{\ell m} \tag{A8}$$

(ix) Liquid slag/plate interface, KJIL plane:

$$T = T_{\ell m} \tag{A9}$$

(x) Vertical surface of the plate QRJK plane:

$$K \frac{\partial T}{\partial y} = \sigma F_{s \to \blacksquare} (\varepsilon_{s\ell} T^4_{s\ell av} - \varepsilon T^4) - h_c (T - Ta) \tag{A10}$$

Where σ is the Stephen-Boltzman constant, $F_{s \to \blacksquare}$ is the view factor, and $T_{s\ell av}$ is the average temperature of the top slag surface.

List of Symbols

C_p - Specific heat of the material of the base plate, kJ/kgK

hc - Heat transfer coefficient at the base plate surface, kJ/m^2sK

$H_{s\ell p\ell}$ - Total amount of heat transported from the liquid slag to the base plate, kH/s

k - Thermal conductivity, kJ/msK

m - Electrode melting rate, kg/s

m_b - Melting rate of the base plate, kg/s

t - Time, s

T, Ta, $T_{\ell m}$ - The symbol T refers to temperature in the computation domain; subscripts a and ℓm refer to ambient temperature and the melting point of metal, K

x, y, z - Distance coordinates, m

ρ - Density, kg/m^3

$\epsilon_{s\ell}$ - Emissivity of the slag surface

ϵ - Emissivity of the base plate

ϕ - Updated value of voltage

ϕ_{old} - Value of voltage prior to iteration